Materials & Design 205 (2021) 109719

Contents lists available at ScienceDirect

Materials & Design

journal homepage: www.elsevier.com/locate/matdes

On the use of laser-scanning vibrometry for mechanical performance evaluation of 3D printed specimens

Francisco Medel [a,*], Víctor Esteban [b], Javier Abad [a]

[a] Department of Mechanical Engineering, Institute of Engineering Research of Aragón-I3A, Campus Río Ebro, School of Engineering and Architecture, Universidad de Zaragoza, Zaragoza, Spain
[b] Technical Department TJF S.A. Caspe, Zaragoza, Spain

HIGHLIGHTS

- Laser-scanning vibrometry successfully discriminated the mechanical behavior of 3D printed specimens produced with different process parameter combinations.
- Equivalent Elastic Modulus data served to confirm significant influences and interactions between process parameters.
- A model was developed to provide elastic modulus values for use in dynamic behavior simulations of 3D printed parts.

GRAPHICAL ABSTRACT

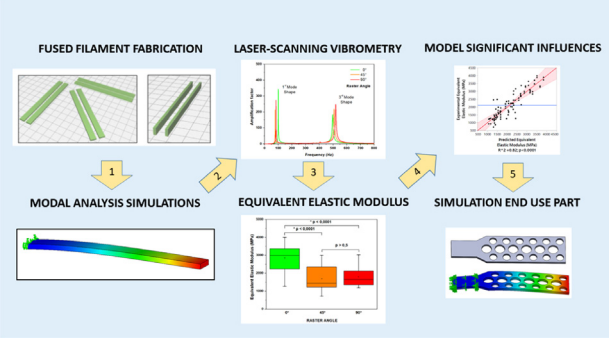

ARTICLE INFO

Article history:
Received 6 November 2020
Revised 28 March 2021
Accepted 7 April 2021
Available online 22 April 2021

Keywords:
Fused Filament Fabrication
3D printing
Laser-scanning vibrometry
Mechanical properties
Elastic Modulus
Polylactic acid (PLA)

ABSTRACT

In this study, we explored the suitability of laser-scanning vibrometry (LSV) for evaluation of the mechanical behavior of rectangular prisms produced by Fused Filament Fabrication (FFF). Our hypothesis was that LSV would be able to discriminate the mechanical behavior of specimens fabricated with different process parameters combinations. Build orientation, raster angle, nozzle temperature, printing speed and layer thickness were the process parameters of interest. Based on a factorial design of experiment approach, 48 different process parameter combinations were taken into account and 96 polylactic acid (PLA) rectangular prisms were fabricated. The characterization of their dynamical behavior provided frequency data, making possible the computation of an equivalent elastic modulus metric. Statistical analysis of the equivalent elastic modulus dataset confirmed the significant influences of raster angle, build orientation and nozzle temperature. Moreover, multivariate regression models served to rank, not only the significant influences of individual process parameters, but also the significant quadratic and cubic interactions between them. The previous knowledge was then applied to generate an ad hoc model selecting the most important factors (linear and interactions). The predicted equivalent elastic moduli provided by our ad hoc model were used in modal analysis simulations of both 3D printed rectangular prisms and a complex part. The simulated frequencies thus obtained were generally closer to the experimental ones ($\leq$11%), as compared to modal analysis simulations based on internal geometry modelling ($\leq$33%). The use of LSV appears very promising in the characterization of the mechanical behavior and integrity of 3D printed parts. Other additive manufacturing technologies may benefit from the use of this technique and from the adoption of the presented methodology to test, simulate and optimize the properties of 3D printed products.

* Corresponding author.
E-mail address: fjmedel@unizar.es (F. Medel).

https://doi.org/10.1016/j.matdes.2021.109719
0264-1275/

1. Introduction

Since the 1980s, Fused Filament Fabrication (FFF), also known as Fused Deposition Modelling (FDM), a trademark registered by Stratasys, has become a very popular additive manufacturing (AM), or 3D printing, technology [1–4]. FFF builds parts by depositing filaments of thermoplastic polymers, previously heated near the melt and extruded through a nozzle, onto a building platform. In this way, parts are produced in a layer-by-layer fashion and each of these layers is composed of a number of filaments or rasters that join to the adjacent ones upon solidification. As an AM technology, FFF allows for fabrication of parts with complex geometries, requires no part-specific tooling, reduces material waste and diminishes fabrication times in the case of short series, as opposed to classic subtractive manufacturing technologies. In the last years, some FFF machines have incorporated two extruders, making possible the use of support material (typically, polyvinyl alcohol) to create overhanging features or the fabrication of parts with two different materials [5]. All these features make FFF a very attractive technology not only for rapid prototyping (fabrication of presentation or educational models, visual aids, etc.) but also for functional, end-use, parts. Thus, the aerospace, automotive and biomedical industries, among others, have incorporated FFF, as well as other AM techniques, to their technological core [6–10].

In the previous context, the mechanical performance of parts fabricated by 3D printing technologies, FFF among them, has been one of the main concerns of the scientific community. Obviously, the mechanical properties of 3D printing materials are paramount when they are intended to produce end use parts. Nevertheless, the mechanical strength of 3D printed parts depends not only on the 3D printing material and technology used, but also on the printing process itself. The choice of a specific combination of printing parameters defines a distinct mechanical behavior. Moreover, it also defines other properties, such as surface roughness, resolution or dimensional accuracy, which may have an impact on mechanical performance via stress concentration effects and other phenomena [11]. Therefore, the properties of parts produced by FFF depend on both the polymeric material of choice and the combination of production process parameters [12,13]. Overall, polylactic acid (PLA) and acrylonitrile butadiene styrene (ABS) are the most popular materials for FFF, although polycarbonate (PC), polyethylene terephthalate (PET), thermoplastic polyurethane (TPU) and polyvinyl alcohol (PVA) are also commonplace. Moreover, composites and high performance polymers, such as poly-ether-ether-ketone (PEEK) or polyetherimide (PEI), are also available for AM, including selective laser sintering and FFF [7–9]. Regarding process parameters, a set of numerous variables, which can be custom adjusted to achieve the desired 3D printed product, characterizes FFF. Thus, bead width (width of a single deposited filament), air gap (the distance between adjacent filaments within a layer), layer thickness (the height of a layer, which is defined by the filament height), raster angle (the in-plane angle between the deposited filament and the building platform), build orientation (orientation of layers with respect to the part to be produced), feed rate or printing speed (i.e. extrusion and deposition velocity), nozzle temperature, envelope or bed temperature, infill density and infill pattern, among others, come into play and may have a relevant impact on the mechanical properties and overall quality of the end product. Furthermore, the anisotropic mechanical behavior of 3D printed parts stems from the very nature of additive manufacturing technologies [14], and, as a multiparametric problem, it is not yet fully understood.

There exists a growing body of scientific literature dealing with the mechanical properties of parts fabricated by FFF, as reviewed by different researchers [15–17]. Most of the reviewed studies focused on the influence of process parameters combinations on static mechanical properties of 3D printed parts, being tensile, compressive and flexural behavior the usual target properties [5,12,13,18–28]. As the main findings, these studies highlight the mechanical anisotropy of parts produced by 3D printing and the strong impact of build orientation, as production of specimens with layers perpendicular to the loading direction resulted in the lowest strength and stiffness performances [12,13,18,19,23,25]. Similar to the build orientation effect, some studies confirm the influence of raster orientation (raster angle) on mechanical behavior depending on whether the deposited filaments or fibers were aligned with the stress axis [22,23,25,26]. In addition, the influence of infill density has been confirmed, with higher infill densities associated with superior mechanical properties [13,27,29,30]. The role of air gap is also clear, with zero or negative air gaps preferred for optimal mechanical properties [12,22,23,29]. In contrast, the effect of other print parameters, such as extrusion temperature, bed temperature, printing speed or layer thickness appear to be more controversial. Thus, some authors point out that higher extrusion temperatures may favor inter-fiber bonding and porosity reduction in 3D printed parts, therefore improving their mechanical properties, particularly fracture resistance [20,31]. However, Abbot and coworkers indicate that extruder temperature played a minor role compared to printing speed in tensile strength and contact length of 3D printed ABS coupons [21], whereas Yin and colleagues found that building stage temperature significantly improved the interfacial bonding strength between TPU and ABS, but nozzle temperature and printing speed had minor influences [5]. Regarding layer thickness, apparently contradictory results have been reported. In this sense, Chacón and coworkers point out that layer thickness had a slight effect on the tensile and flexural strength of specimens printed on flat and on edge, while higher layer thicknesses increased the corresponding properties for upright samples [18]. Rodríguez Panes and collaborators conclude that increased layer height diminishes tensile strength [13]. Sood and colleagues remarked that low layer thickness is connected to a higher number of layers, fact that may imply better diffusion and bonding in bottom layers, but also a higher number of heating and cooling cycles that could generate residual stresses in the part [22]. Moreover, Gómez-Gras and coworkers identified an interaction between nozzle diameter and layer height and predicted a detrimental fatigue performance when both parameters take a similar value [30]. In this sense, Aliheidari and colleagues reported a huge rise in fracture resistance when layer height was decreased from 0.3 to 0.2 mm for a 0.35 mm nozzle diameter, but this effect was partially lost for the lowest layer thickness, namely 0.1 mm [31]. Very recently, Basgul and collaborators have explored the effects of printing speed, post-processing annealing and alteration of layer cooling times on the mechanical properties of 3D printed PEEK lumbar cages [7–9]. The conclusions of these researchers were, on one hand, that printing speed was an important parameter for 3D printed-PEEK, whereas annealing did not produce markedly better mechanical (compression and torsion) properties, but a slightly more noticeable effect was found at lower printing speeds [7,8]. On the other hand, the alteration of layer cooling by using bigger nozzle diameters and printing one cage at a time was an effective strategy to improve mechanical properties (compression) of 3D printed PEEK cages [9]. Altogether, these studies reflect the complexity of the mechanical performance of 3D printed parts, pointing out that, not only the influence of individual factors, but also interactions between process parameters may take place and have significant effects on the final mechanical properties. Although interfacial contact and intermolecular diffusion, which are thermally driven phenomena, govern neck-growth and inter-fiber bonding of 3D printed parts [32], and there-

fore their mechanical properties, the control of these physical phenomena by properly combining process parameters remain to be fully understood.

In contrast to static mechanical properties, there is a lack of knowledge about the dynamic behavior of parts produced by FFF. Mohamed and coworkers studied the dynamic mechanical behavior of 3D printed specimens [33]. They observed that both storage and loss compliances were more sensitive to layer thickness, air gaps and number of perimeters. Specifically, they found the highest storage and loss compliances for the lowest layer thickness, positive air gaps and the lowest number of perimeters, due to the increased number of layers and the associated formation of micro-voids, the absence of bonding between rasters and the comparatively weaker part walls, respectively. Lee and Huang and Ziemian and colleagues have pioneered the study of fatigue behavior of additively manufactured ABS parts [23,24,34]. Lee and Huang remarked the limited fatigue characteristics of FDM ABS parts, although they exhibited similar ultimate stress limits than bulk materials [34]. Ziemian and collaborators reported the superiority of the 45°/−45° infill pattern in fatigue endurance and a three stages fatigue damage model for 3D printed ABS specimens [24]. In this model, the rapid growth of fatigue damage (crazing, delamination and fiber cracking) at the first stage of fatigue life preceded a steady and slowest increase in the second stage that make way to rapid damage in the final stage. More recently, Gomez-Gras and coworkers have proposed honeycomb infill patterns, 75% infill density, 0.5 mm nozzle diameter and 0.3 mm layer height for optimal rotating bending fatigue performance [30]. As far as creep properties are concerned, Salazar-Martín and Turk have studied the creep behavior of additively manufactured specimens, concluding that creep strain increases when air gap increases or the number of contours decreases and the flexural creep modulus decreases with temperature, respectively [29,35]. Regarding vibration behavior, to the authorś knowledge only few studies have employed laser-scanning vibrometry to assess the mechanical performance of 3D printed structures or products [10,36,37]. Boldrin and colleagues used laser-scanning vibrometry to assess the vibroacoustic response of 3D printed auxetic gradient honeycomb composite structures [10]. Kozin and coworkers created tympanic membrane grafts by multi-material 3D printing and employed laser Doppler vibrometry to measure surface motions in response to sound [36]. Filippov et al attributed the differences in oscillation frequencies, vibration velocities and damping factors to the presence of numerous defects homogeneously distributed in 3D printed carbon fiber composites [37]. In view of these studies, the use of laser-scanning vibrometry might add significant knowledge about the mechanical performance of 3D printed parts. Regarding FFF, the number of filaments and layers used to produce a part, as well as the bonds generated between them, will be responsible for a distinct vibration behavior, which depends on part stiffness. Typically, lower numbers of filaments and layers, as well as bonds between them, are expected to result in lower part stiffness. Another advantage of laser-scanning vibrometry is its non-destructive and non-invasive nature, making this technique an attractive candidate to assess the mechanical integrity and quality of parts obtained by FFF.

In the present paper, our objective was to confirm the suitability of laser-scanning vibrometry for mechanical performance characterization of specimens produced by FFF. We hypothesized that laser-scanning vibrometry would be able to discriminate the mechanical behavior of 3D printed specimens fabricated with different process parameters combinations. Moreover, laser-scanning vibrometry would serve to rank the influence of individual process parameters as well as to detect interactions between them. For this purpose, and based on a factorial design of experiment approach, a set of specimens was fabricated by FFF for further vibrational characterization. Forty-eight different process parameters combinations were taken into account, including build orientation, raster angle, layer thickness, nozzle temperature and printing speed as the main 3D printing parameters. The modal analysis of the 3D printed rectangular prisms (n = 96) was carried out paying attention to the equivalent elastic modulus as target property. A multivariate regression analysis of the vibrational data was performed to identify and rank significant factors and interactions between the previous 3D printing process parameters. Finally, simulations of the dynamic behavior of 3D printed specimens were carried out to test the utility of the equivalent elastic modulus metric obtained from the laser-scanning vibrometry.

2. Materials and methods

2.1. 3D printing fabrication

Rectangular prisms (90 × 7 × 2 mm^3) were designed using the Computer Aided Design (CAD) software Solid Works (Dassault Systèmes; Paris, France). The slicing software Cura (Ultimaker BV; Utrecht; Netherlands) served to convert STL files generated in Solid Works into G-code files and specimens were fabricated from them using a commercial 3D printer Ultimaker 3 Extended (Ultimaker BV; Utrecht; Netherlands). 2.85 mm diameter PLA filament spools (Ultimaker BV; Utrecht; Netherlands) and a nozzle of 0.4 mm were employed. Based on a factorial design of experiments (DOE) approach, a sample set of n = 96 specimens was generated considering layer height, build orientation, nozzle temperature, raster angle and printing speed as 3D printing process parameters. Two levels for each of the selected 3D printed parameters, three levels in the case of raster angle, were considered (see Table 1). Thus, 48 different combinations of 3D printing process parameters were taken into account and two specimens were fabricated for each parameter combination, giving the 96 specimens.

Although the slicing software Cura allows control of almost 500 individual printing parameters, most of them were not considered as variables in the present study. When needed, they were set to default values, for instance, the height (0.2 mm) and printing speed (40 mm/s) of the initial layer, bed temperature (70 °C), travel speed (250 mm/s) and infill density (100%), among others. Typically, specimens built on flat were fabricated in six-samples printing batches, whereas specimens built on edge were produced in two-samples printing batches (Fig. 1). Upon fabrication, specimens were measured in three different points to register their average nominal dimensions, which allowed computation of a volumetric

Table 1
3D printing process parameters considered in the present study.

3D Printing parameters										
Build Orientation		Layer height (mm)		Nozzle Temperature (°C)		Printing Speed (mm/s)		Raster angle (°)		
On flat	On edge	0.1	0.25	200	220	60	120	0	45	90

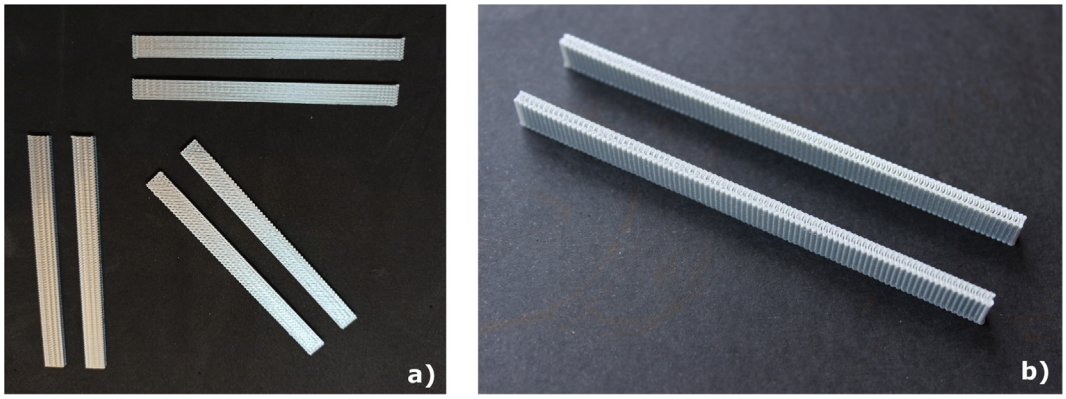

Fig. 1. 3D printed rectangular prisms built on flat, a), and built on edge, b).

error (in percentage), as a difference between the nominal and theoretical volumes.

2.2. Experimental analysis of dynamical behavior of 3D printed specimens

The characterization of the dynamic behavior of 3D printed specimens entailed obtaining their Transmissibility Frequency Responses based on a cantilever beam configuration. Thus, the target property was the amplification factor between the excitation at the fixed end of the specimen and the vibratory response at its free end for every tested frequency. For this purpose, a 3D printed rectangular prism was clamped to a 2075 E shaker (The Modal Shop; Cincinnati, Ohio), leaving 70 mm of free length as cantilever beam. Then, dynamic tests were carried out subjecting specimens to a random broadband excitation, which had a value of $((0.05\ m/s^2)^2)/Hz$ and covered a range from 10 to 1000 Hz, at the fixed end. A T333B30 accelerometer (PCB; Depew, New York) served to control the input vibration signal, which sought stimulation of the out-of-plane bending vibration modes. As the specimen mass was small, laser Doppler vibrometry was performed to measure the vibration response at the free end using a PDV10 laser vibrometer (Polytec; Waldbronn, Germany). A PULSE^{TM} system (Brüel&Kjaer; Nærum, Denmark), which consists of a data acquisition front-end (Type 3560-C) and the PULSE software version 9.2, allowed registration and digital processing of the signals. Furthermore, it provided the Transmissibility Frequency Response Function for each specimen based on the Fast Fourier Transform analysis of the signals with 6400 lines of resolution, an analysis range from 0 to 800 Hz, and averaging a hundred temporal measurements with an overlap of 66.67%. Amplification factor versus frequency plots, generated using the vibration response data, allowed for identification of the natural frequencies that correspond to amplification factor maxima.

The solution to the equation of motion of a solid, continuous and uniform, cantilever beam subjected to free lateral vibration gives the natural frequencies of the different vibration modes, according to the following formula [38]:

$$f_i = \sqrt{\frac{E \cdot J}{\rho \cdot A}} \frac{1}{2\pi} \left(\frac{k_i}{l}\right)^2 \tag{1}$$

where f_i is the natural frequency of the considered vibration mode, E denotes the elastic modulus of the material, k_i are constants related to the vibration mode (1.875 for the first vibration mode) and ρ is the density of the material. A, l and J are the cross-sectional area of the beam, free length and the moment of inertia of the beam cross section, respectively.

Based on the previous equation and the experimental characterization of modal behavior, an elastic modulus metric was computed for every 3D printed rectangular prism using the next formula [38,39]:

$$E = \left(\frac{f_i \cdot 2\pi}{\left(\frac{k_i}{l}\right)^2}\right)^2 \cdot \frac{\rho \cdot A}{J} \tag{2}$$

In the case of our 3D printed, partially solid, rectangular prisms, this elastic modulus metric did not represent the elastic modulus of the material, but an equivalent elastic modulus that results from the contributions of the deposited filaments and the bonds between them, which have different elastic moduli.

2.3. Statistical analysis

The influences of 3D printing parameters on the vibrational properties of rectangular prisms were statistically analyzed using JMP 13 software (SAS Institute; Cary, North Carolina). To examine the influence and effects of 3D printing parameters on the dynamic behavior, box plots of volumetric error and equivalent elastic modulus versus a specific 3D printing process parameter were prepared. The normality of data groups was confirmed (or rejected) by the Shapiro-Wilk test. Student t-tests or Wilcoxon tests served to confirm significant differences between means of normally or non-normally distributed data groups, respectively (level of significance $p < 0.05$). In addition, the regression analysis platform of JMP 13 software allowed us to generate multivariate regression models for the target property, namely the equivalent elastic modulus of the 3D printed parts, as functions of the input parameters, that is the 3D printing process parameters. In these models, the influences of individual factors (factor 1, factor 2, factor 3 ...) as well as those of potential quadratic (factor1*factor2 ...) and cubic (factor1*factor2*factor3 ...) interactions were taken into account.

2.4. Numerical analysis of dynamical behavior of 3D printed samples

Simulations of the dynamic behavior of rectangular prisms were carried out using Solid Works (Dassault Systèmes; Paris, France). First, modal analysis simulations of a solid rectangular prism with a fixed end provided the mode shapes and the corresponding natural frequencies, using a standard mesh and an element size of 0.4 mm. In this case, an elastic modulus value of 2346.5 MPa was used for PLA. Afterwards, modal analysis simula-

tions were performed using the equivalent elastic moduli obtained in the experimental characterization. Finally, modal analysis simulations based on the internal geometry of 3D printed rectangular prisms were conducted. To design partially solid 3D printed specimens fabricated at 0°, 45° and 90°, our strategy was to draw a solid rectangular prism, from which some material was removed extruding 0.01 mm thick holes at the corresponding angle and without reaching the external walls of the specimen. Thus, filaments of about 0.4 mm in diameter were indirectly created (Fig. 2). Simulations were performed selecting a curvature-based mesh with an element size of 0.1 mm. This design strategy allowed successful modal analysis simulations using Solid Works. Simulations based on individual filaments were discarded, as they were computationally very expensive. Finally, a more complex part, a multi-tube support, was designed and, then, simulation of its dynamic behavior was carried out, using both the nominal elastic modulus of PLA (2346.5 MPa) and the equivalent elastic modulus of the part according to its 3D printing design parameters. Moreover, this part was 3D printed and tested to compare its experimental dynamic behavior with the previous simulation. In general, all the simulations of the vibrational behavior focused on the frequency of the first mode shape.

3. Results and discussion

3.1. 3D printing fabrication and dimensional accuracy

3D printing process parameters clearly influenced the final dimensions of the rectangular prisms. Thus, fabrication performed selecting 0° as raster angle yielded significantly lower volumetric errors, averaging a 6 ± 4% (n = 32), as compared with parts fabricated with 45° or 90°, which averaged 17 ± 8% (n = 32) and 18 ± 9%, respectively ($p < 0.0001$ in both cases; Wilcoxon test; see Fig. 3a). Similarly, the on flat build orientation was associated with significantly lower volumetric errors ($p < 0.002$; Wilcoxon test; see Fig. 3b). On average, the volumetric error for specimens fabricated on flat (n = 48) was 10 ± 2%, whereas this property increased up to 18 ± 12% in the case of parts printed on edge. The remaining 3D printing process parameters exhibited no significant influences regarding dimensional accuracy within the ranges considered in this study ($p > 0.17$; Wilcoxon tests).

The influence of build orientation on part accuracy was expected, as Ahn and coworkers mentioned it in their build rules. They noticed that two-dimension slices closely reproduce geometry, whereas three-dimension layer stacking creates linear approx-

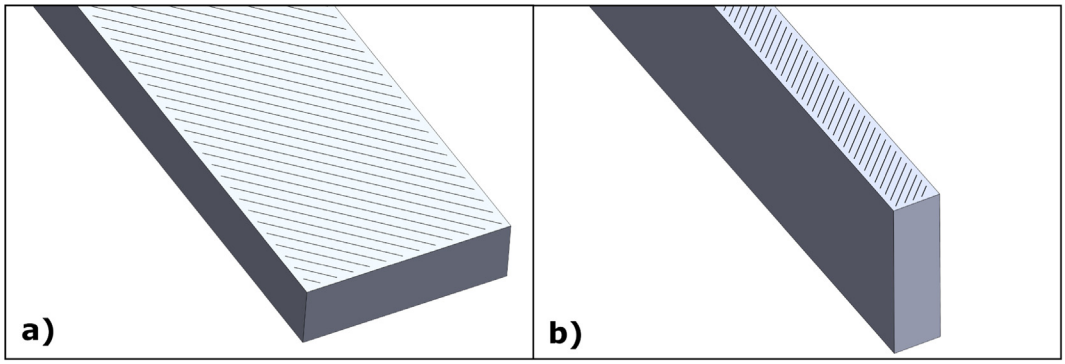

Fig. 2. Schematics of the internal geometry modelling of rectangular prisms printed at 45° on flat, a), and on edge, b).

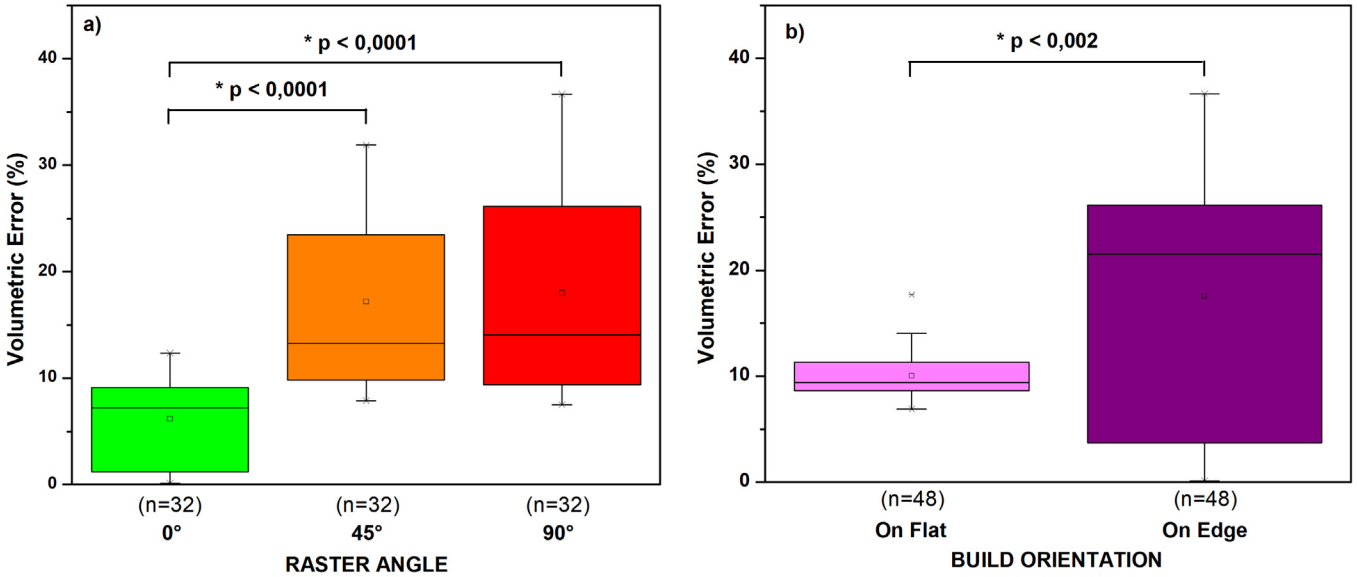

Fig. 3. Volumetric error of rectangular prisms fabricated at different raster angles, a), and build orientations, b).

imations [12]. In our study, the geometrical dimensions of the specimen clearly affect the value of equivalent elastic modulus (see Eq. (2)) and therefore it is necessary to control part accuracy in FFF to obtain the actual mechanical performance. Furthermore, FFF inherently generates a characteristic mesostructure in 3D printed parts, featuring voids and interlayer necks [31]. In the present study, we did not account for mesostructure, which would have provided more accurate cross sectional area and moment of inertia values. Nevertheless, the focus of our study was not to characterize the mesostructure of 3D printed specimens, but to obtain a metric from laser-scanning vibrometry experiments that would capture the mechanical behavior of 3D printed specimens produced using different process parameter combinations and, therefore, featuring different mesostructures.

3.2. Numerical and experimental analysis of dynamical behavior

As a preliminary study, we performed a simulation of the dynamic behavior of a solid rectangular prism in a cantilever beam configuration. This simulation returned the modes shapes and their corresponding frequencies for this sample. The first vibration mode was a vertical (out-of-plane) bending found at a frequency of 91.2 Hz. The remaining mode shapes were a horizontal (in-plane) bending at 315 Hz (second mode), a double vertical bending at 569 Hz (third mode), a torsion at 1488 Hz (fourth mode), and a triple vertical bending at 1584 Hz (fifth mode; see Fig. 4).

3.3. Experimental analysis of dynamical behavior of 3D printed samples

3.3.1. Frequency

Laser Doppler vibrometry was able to discriminate the dynamic behaviors of rectangular prisms fabricated with different 3D printing parameters combinations. Thus, amplification factor-frequency plots revealed differences in both frequency and amplification factor magnitude behavior depending on the 3D printing fabrication conditions (representative amplification factor-frequency plots are shown in Fig. 5). As far as frequency is concerned, parts printed on edge (n = 48) had significantly higher frequencies for the first mode shape, averaging 102 ± 18 Hz, against specimens fabricated on flat, which reached an average frequency of 79 ± 13 Hz ($p < 0.0001$; Wilcoxon test; see Table 2). Likewise, the highest nozzle temperature was associated with significantly higher frequencies (n = 48; 95 ± 18 Hz; $p < 0.007$; Wilcoxon test). In addition, significantly lower frequencies were registered for specimens fabricated with a raster angle of 45° (n = 32; 85 ± 23 Hz) in comparison with samples printed at 0° (n = 32; 96 ± 15 Hz; $p = 0.02$; Wilcoxon test).

3.3.2. Influence of 3D printing process parameters on the equivalent elastic modulus

The experimental dynamic data along with the measured dimensions of the rectangular prisms allowed for computation of equivalent elastic moduli. Overall, raster angle was the most signif-

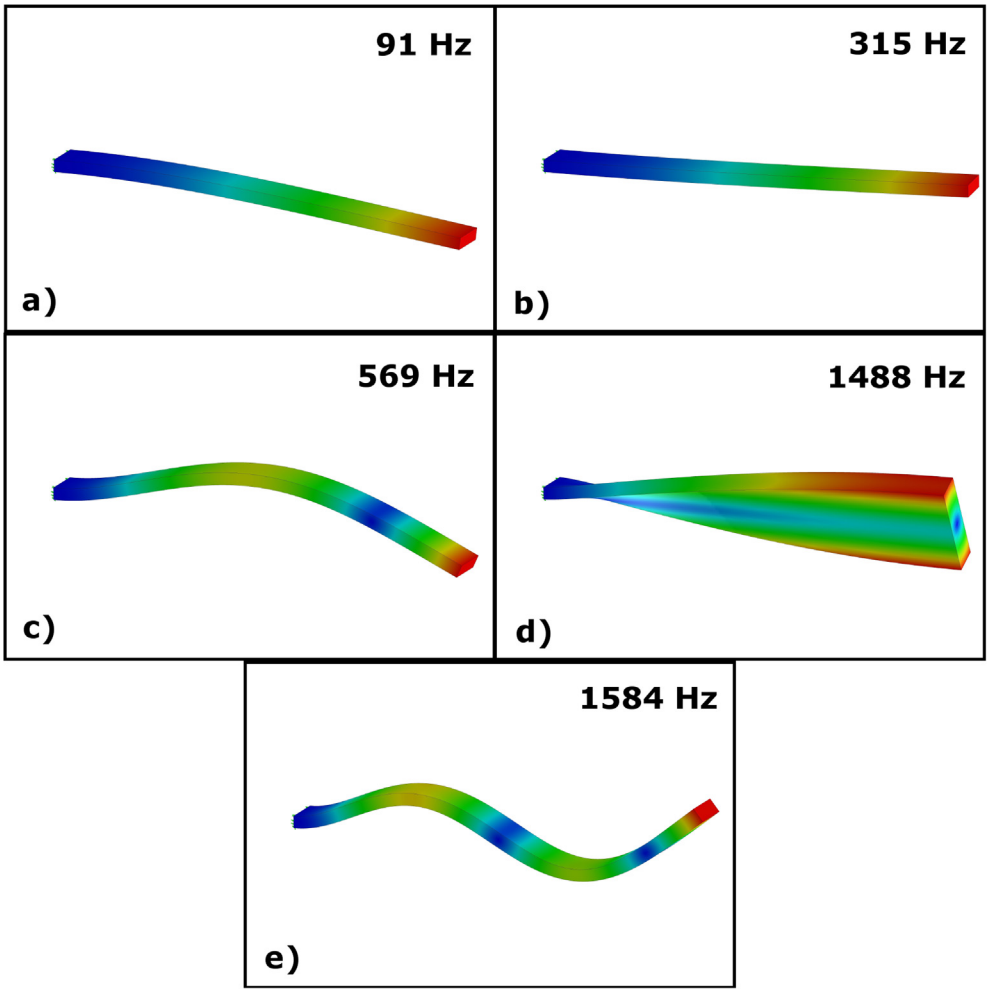

Fig. 4. Simulated mode shapes and their corresponding frequencies for a solid rectangular prism.

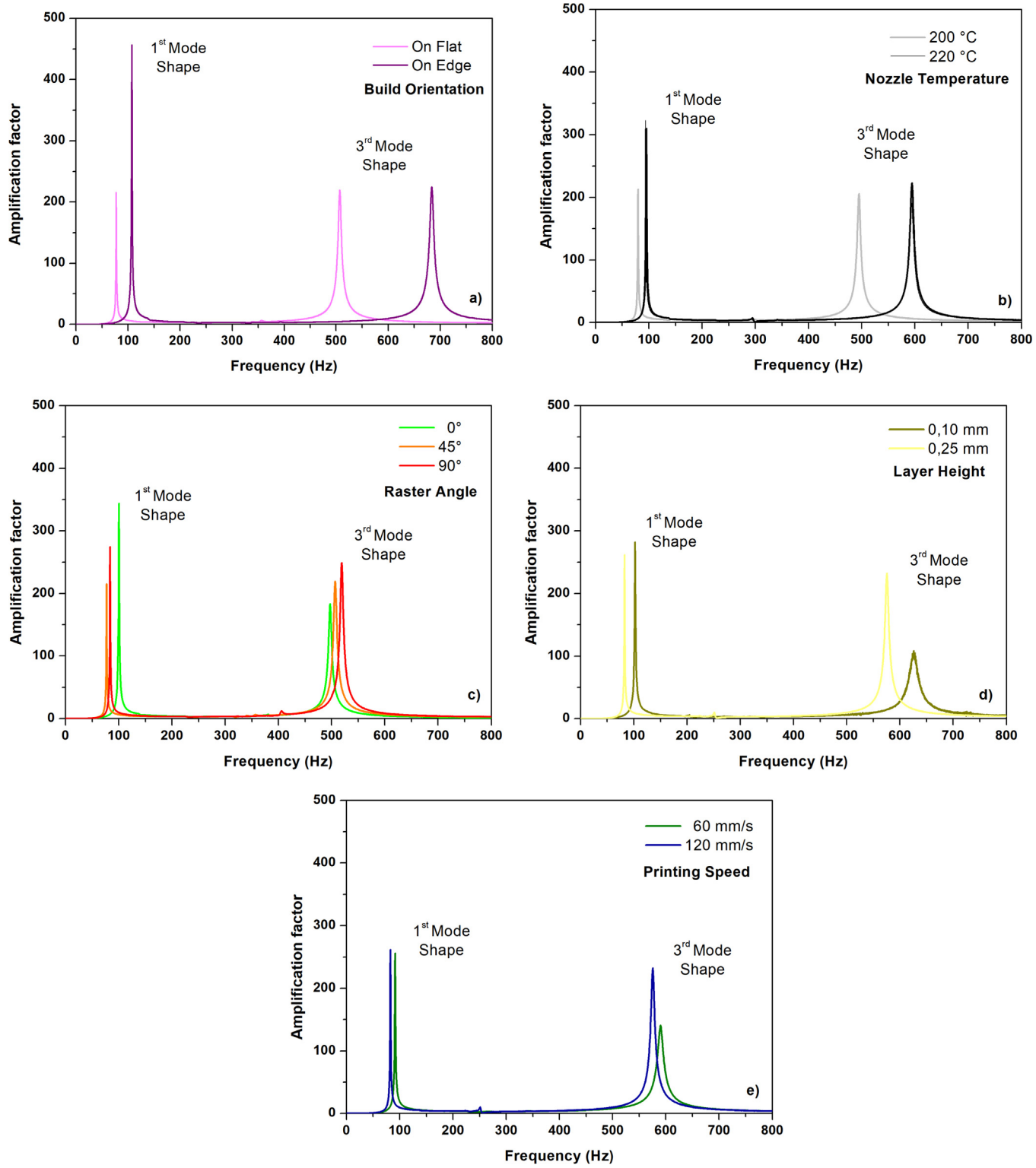

Fig. 5. Representative amplification factor versus frequency plots of rectangular prisms fabricated under different 3D printing conditions: build orientation, a), nozzle temperature, b), raster angle, c), layer height, d), and printing speed, e).

icant factor of the 3D printing process regarding stiffness behavior (see Fig. 6a). Thus, parts printed at 0° (n = 32) exhibited significantly higher elastic moduli (2856 ± 766 MPa) as compared with specimens printed at 45° (n = 32) and 90° (averaging 1695 ± 684 and 1802 ± 475 MPa, respectively; $p < 0.0001$ in both cases; Wilcoxon and Student's *t*-test, respectively; see Table 2). However, no significant differences were detected between equivalent elastic modulus of parts printed with raster angles of 45° and 90° ($p = 0.2$; Wilcoxon test).

Sood and coworkers highlighted the importance of raster angle in the strength of parts manufactured by FFF [22]. In their work, small raster angles implied longer rasters aligned to the loading

Table 2
Frequency and equivalent elastic modulus data of 3D printed rectangular prisms grouped by the process parameters of interest.

	3D Printing parameters										
	Build Orientation		Layer height(mm)		Nozzle Temperature(°C)		Printing Speed (mm/s)		Raster angle(°)		
	On flat (n = 48)	On edge (n = 48)	0.1 (n = 48)	0.25(n = 48)	200 (n = 48)	220 (n = 48)	60 (n = 48)	120 (n = 48)	0 (n = 32)	45 (n = 32)	90 (n = 32)
Frequency (Hz)	79 ± 13	102 ± 18	92 ± 23	88 ± 16	85 ± 20	95 ± 18	90 ± 19	90 ± 21	96 ± 15	85 ± 23	90 ± 19
Equivalent Elastic Modulus(MPa)	1866 ± 697	2369 ± 889	2158 ± 858	2078 ± 816	1905 ± 801	2331 ± 819	2150 ± 887	2085 ± 785	2856 ± 766	1695 ± 684	1802 ± 475

direction, therefore resulting in strength improvement. Other studies reported similar findings, connecting small raster angles with higher ultimate and yield tensile strengths and elastic modulus, as long as the deposited fibers were aligned to the stress axis [12,23,26]. In our study, the first mode shape corresponds to a flexural mechanical scenario and the smallest raster angle (0°) implies bending of fibers favorably aligned to the stress configuration. In addition, our equivalent elastic modulus results for higher raster angles (45° and 90°) agree with the elastic modulus behavior reported by Casavola and colleagues, who pointed out similar elastic moduli for these raster angles [26].

Build orientation also had a significant effect on the elastic modulus, as specimens fabricated on edge (n = 48) showed significantly higher equivalent elastic moduli (2369 ± 889 MPa; $p < 0.006$; Wilcoxon test; Fig. 6b). Nozzle temperature also demonstrated a significant influence on the elastic modulus, with the highest nozzle temperature (220 °C) associated with higher elastic moduli (n = 48; 2331 ± 819 MPa; $p < 0.008$; Wilcoxon test; Fig. 6c). In contrast, layer height and printing speed were not significant parameters from the elastic modulus perspective ($p > 0.6$ in both cases; Wilcoxon tests; Table 2). The scientific community completely agrees about the influence of build orientation on mechanical performance of 3D printed parts [12,13,18,19,21,23,25,29,40,41]. In most studies, the upright build orientation implies part production with layers perpendicular to the stress axis, which is the most unfavorable mechanical scenario, as interlayer bonds, not fibers, have to withstand the load. Coherently, the upright build orientation was not included in the present study, but even so, laser-scanning velocimetry was able to detect different mechanical behaviors within specimens fabricated with on flat and on edge build orientations. Our results are in general agreement with the findings reported by Chacón and coworkers, who identified on-edge orientation as the best build orientation for mechanical (strength, stiffness and ductility) performance [18]. As far as nozzle temperature is concerned, this process parameter appeared to have a significant influence on the equivalent elastic modulus of the present 3D printed parts. There is no complete agreement in the scientific community about the influence of extrusion temperature on mechanical properties, as some researchers report a strong effect of this parameter on fracture resistance [31] and other investigators affirm extruder temperature plays a minor role [21]. In our opinion, these apparently contradictory results might stem from the particular temperature values included in each study. Thus, if all the selected temperature levels are above a threshold temperature, the influence of extruder temperature will be insignificant. In this sense, Abbot and collaborators chose two temperature levels, namely 230° and 270°, and they measured the cooling time for 3D printed ABS tensile coupons and, in both cases, the time that bond lines between layers were above glass transition temperature (103.6 °C) was long enough to ensure good adhesion, at least from the uniaxial tension perspective [21]. On the contrary, Aliheidari and coworkers included extruder temperature values as low as 220 °C in their study and, coherently, they found a significant effect of this parameter on the fracture resistance of ABS double cantilever beam specimens [31]. In our study, the selected nozzle temperature levels for 3D printed PLA specimens, equal to or lower than 220 °C, appear to capture this threshold temperature between them, making possible the detection of significant influences. Regarding printing speed, we were not able to detect significant differences in equivalent elastic modulus based on the levels included in our experimental design (60 mm/s and 120 mm/s). Nonetheless, some studies point out the importance of increased local heating from the heated nozzle at low printing speeds (10 mm/s) [21]. This increased local heating effect reflects the importance of cooling times in FFF. In this sense, 3D printing of fewer parts per build implies slower cooling, yielding better mechanical strength as signaled by Basgul and colleagues [9]. In our study, specimens built on edge demonstrated, on average, superior equivalent elastic modulus. In particular, specimens fabricated selecting on edge build orientation; a raster angle of 0°; a nozzle temperature of 200 °C; a layer height of 0.25 mm and a printing speed of 60 mm/s exhibited the highest equivalent elastic modulus (3995 MPa). On-edge specimens were fabricated in two-parts builds and based on narrower layers. Both facts contributed to make layer deposition comparatively faster, so the next layer was deposited while the temperature of the previous one was relatively high. Moreover, local heating effects, due to the proximity of the extruder hot end, also had a relevant influence in this case. Therefore, cooling times were comparatively longer for rectangular prisms built on edge, favoring crystallization of both fused filaments and regions of inter-filament bonding [32]. In this sense, Sarasua and colleagues suggested that more crystalline and stiffer PLA materials developed at lower cooling rates [42]. The noticed mechanical improvement in our study might also reflect that enhanced crystallization via slow cooling plays an important role in FFF, counteracting the negative effects of too low extruder temperatures or even too high printing speeds. Finally, layer thickness had no significant effects on the present equivalent elastic modulus results. Again, the inclusion of more layer thickness levels in the experimental design might unveil significant effects, especially at higher layer thicknesses (0.3 mm and above), for which smaller contact areas between deposited filaments and inferior adhesion are anticipated [31].

To confirm our experimental dataset (n = 96) had adequate power to detect significant differences in equivalent elastic modulus provoked by changes in process parameters, a power analysis was performed (level of significance $p < 0.05$). Thus, a power of 93% to detect a 10% variation (210 MPa) in the equivalent elastic modulus was confirmed for our dataset and model. Further statistical analysis using multivariate regression models provided deeper knowledge about potential influences of 3D printing design parameters on the dynamic behavior of parts fabricated by fused filament fabrication. In general, regression models taking into account only single factors with no interactions (factor 1, factor 2, ... , factor 5) between the 3D printing design parameters did not fit well enough the equivalent elastic modulus data ($R^2 = 0.56$; see Fig. 7a). As far as potential interactions between

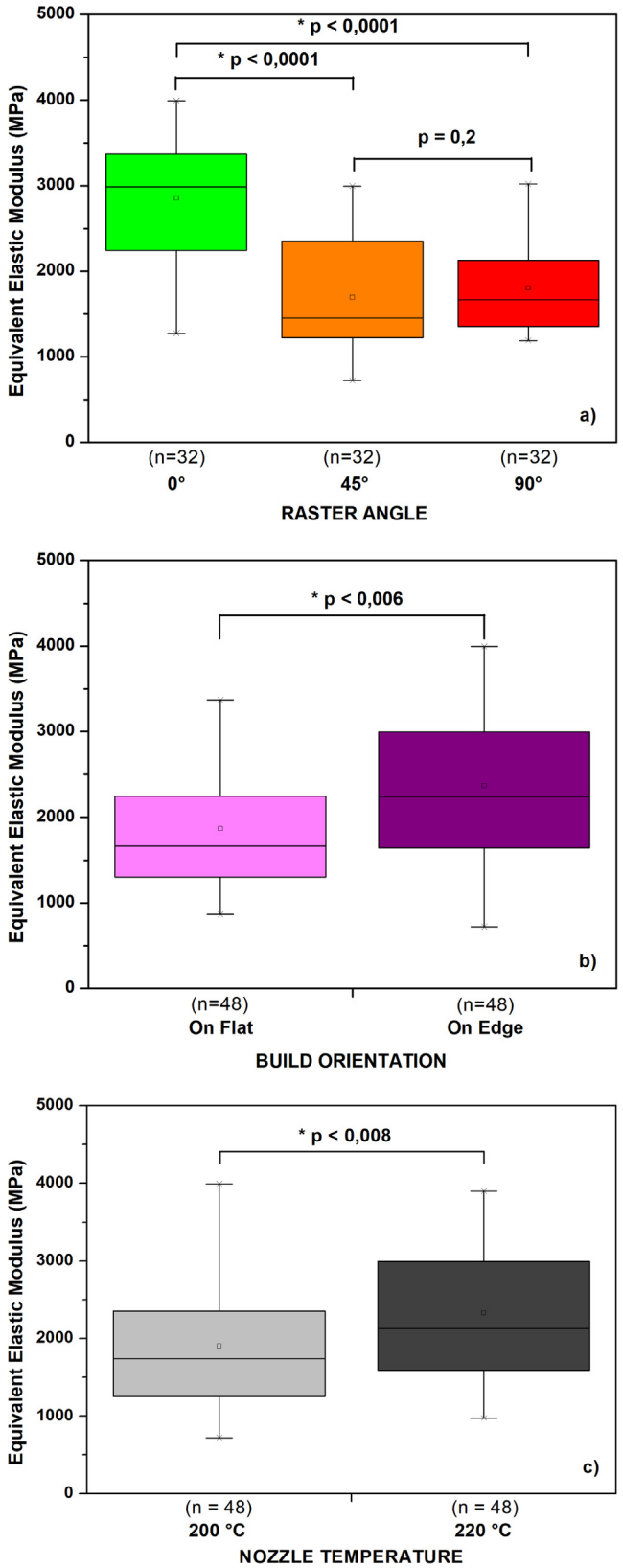

Fig. 6. Influence of 3D printing process parameters on the equivalent elastic modulus of rectangular prisms: raster angle, a), build orientation, b), and nozzle temperature, c).

3D printing parameters, regression models that included quadratic (factor1*factor2, etc.) and cubic interactions (factor1*factor2*factor3, etc.) confirmed significant effects on the equivalent elastic modulus. Thus, the inclusion of quadratic interactions improved the model fit (R^2 = 0.71). Moreover, a further improvement arose when cubic interactions were also considered (R^2 = 0.87; Fig. 7b). The disadvantage of the latter model was the high number of variables, which reached 25. To generate a suitable model for the equivalent elastic modulus without too many variables, an ad hoc model was built, considering the most significant factors (including single factors as well as quadratic and cubic interactions) based on their utility logarithm, which is the negative logarithm of the corresponding p-value (see Table 3).

Therefore, this ad hoc model consisted of 11 elements and reached a reasonably good fit (R^2 = 0.82) with a lower number of variables than models including all the quadratic and cubic interactions. In this model, the single factors raster angle, build orientation and nozzle temperature exhibited the greatest utility logarithms, followed by the quadratic interaction between printing speed and raster angle (in fourth place) and the cubic interaction between build orientation, printing speed and raster angle (fifth place; see Table 3).

Regarding unexpected or hidden interactions between 3D printing fabrication parameters, the interaction graphics shown in Fig. 8 helps to identify potential synergies. For instance, raster angle and printing speed (fourth box in the fifth row) significantly interact, as the equivalent elastic modulus decreased for the highest printing speed at 0° and 90° raster angles, whereas the tendency was the opposite at 45°. On the contrary, raster angle and layer height (second box in the fifth row) did not interact, as the use of different layer heights did not provoke significant changes in the equivalent elastic modulus.

Overall, the statistical analysis of the current equivalent elastic modulus data establishes the hierarchy of 3D printing process parameters from a mechanical perspective. It is noteworthy that not all the process parameters had a linearly significant effect, as printing speed and layer thickness exhibited no significant influences. Moreover, preliminary trials including square terms of all process parameters (for instance, factor 1* factor 1) did not yield better fits for the elastic modulus. In this regard, Lanzotti and coworkers reported layer thickness, infill orientation (i.e. raster angle) and number of shell perimeters were linearly significant for the ultimate tensile strength of ABS coupons, but only the square term of number of shell perimeters was significant [43]. Similar to our statistical results, Lanzotti and collaborators found significant quadratic interactions between different process parameters [43]. Nevertheless, the present multivariate regression models did not account for the entire variability of the equivalent elastic modulus data, missing an 18%. Probably, the addition of more levels in the considered process parameters, as well as consideration of more factors, such as bed temperature, air gap or number of shell perimeters, would improve the goodness of fit. In any case, the utility of any model arises from its simplicity, ease of application and prediction capability. To assess the prediction capabilities of our ad hoc model, a new set of six specimens (validation group) was fabricated based on combinations of 3D printing process parameters not used before (see Table 4) and subsequently tested.

The inclusion of these specimens in the ad hoc model, as well as their corresponding 3D printing design parameters and experimental equivalent elastic moduli, gave a very similar goodness of fit: R^2 = 0.81 (see Fig. 7d). The predicted equivalent elastic moduli for this validation group were lower than the experimental results, averaging a difference of 33 percent (range: 1–65%; see Table 4). The dispersion of these predicted equivalent elastic moduli points out that our ad hoc model did not cover the whole universe of process parameters, interactions and levels. As mentioned, a higher number of data points is needed to achieve more accurate predictions, at the expense of longer experimental times. Nevertheless,

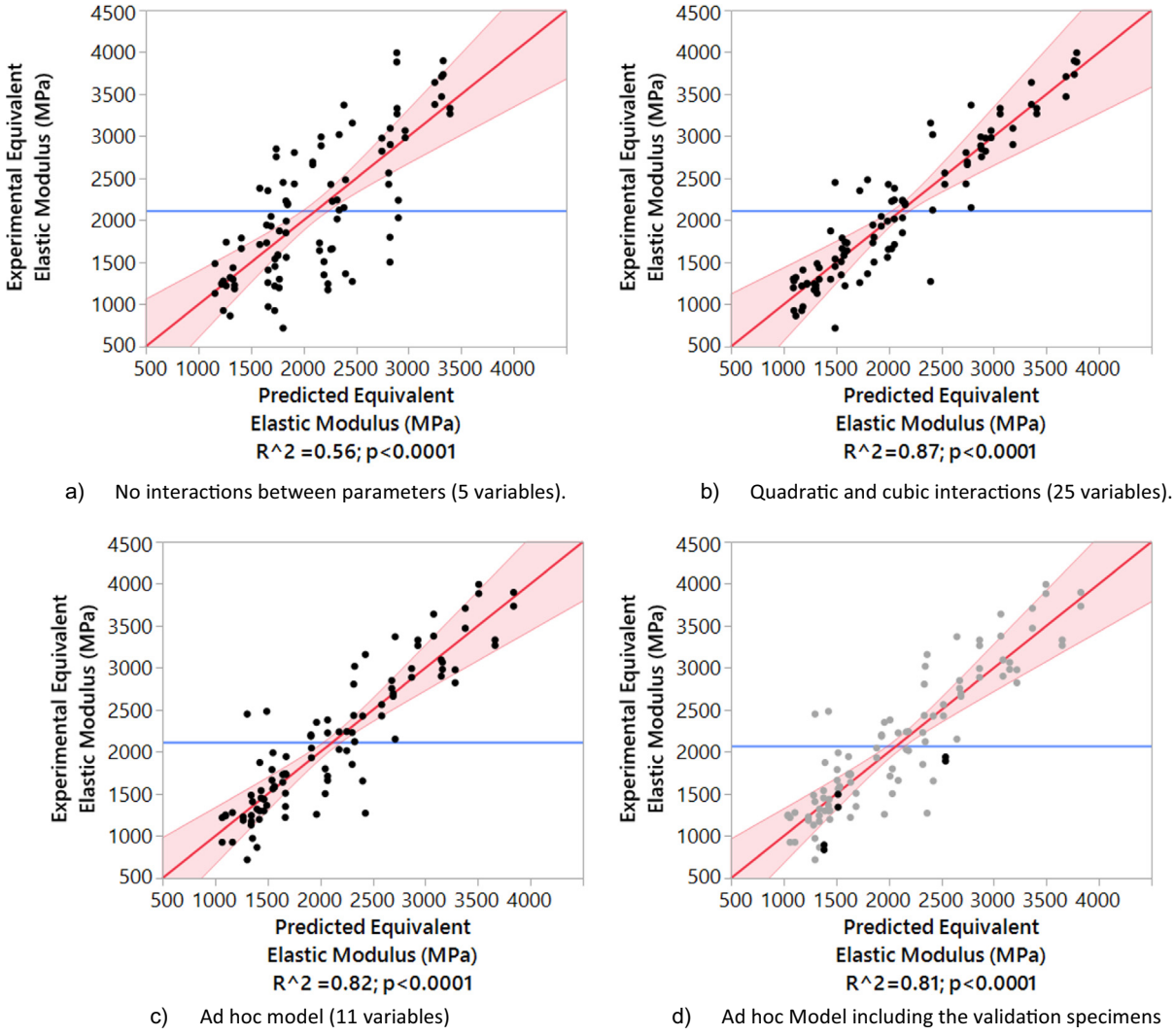

Fig. 7. Multivariate regression analysis models of equivalent elastic modulus data. Model considering no interactions between parameters (5 variables), a), Model including all the quadratic and cubic interactions (25 variables), b), Ad hoc Model including selected quadratic and cubic interactions (11 variables), c), Ad hoc Model including the validation specimen group, d).

Table 3
Significance of individual 3D printing process parameters and their interactions on the equivalent elastic modulus behavior.

3D Printing Process Parameter	Utility logarithm	P-value
Raster angle	18.0	$1.1*10^{-18}$
Build orientation	7.7	$2.2*10^{-8}$
Nozzle Temperature	6.0	$9.6*10^{-7}$
Printing speed*Raster angle	5.9	$1.2*10^{-6}$
Build orientation*Printing speed*Raster angle	4.7	$1.8*10^{-5}$
Nozzle temperature*Printing speed	2.6	$2.8*10^{-3}$
Build orientation*Layer height*Printing speed	2.5	$3.3*10^{-3}$
Nozzle temperature*Raster angle	2.2	$5.7*10^{-3}$
Build orientation*Layer height	2.0	$9.9*10^{-3}$
Layer height*Nozzle temperature*Raster angle	1.9	$1.2*10^{-2}$
Nozzle temperature*Printing speed*Raster angle	1.9	$1.3*10^{-2}$

the use of the predicted equivalent elastic modulus may still be a useful tool in simulations of the dynamical behavior, as shown in the next section.

3.4. Numerical analysis of dynamical behavior of 3D printed samples

Numerical simulations of the dynamic behavior of 3D printed rectangular prisms confirmed the usefulness of the equivalent elastic modulus metric. Thus, simulations of solid rectangular prisms using the equivalent elastic modulus predicted by the ad hoc model captured the experimental dynamic behavior. In these simulations, the mean frequency of all the specimens fabricated with a same 3D printing design parameter combination was the target property. In all cases, the deviation between the simulated and the mean experimental frequency was lower than 12% (see Table 5).

Regarding simulations of the dynamic behavior modelling the internal geometry of the specimens, the simulated frequencies remarkably deviated from the experimental frequencies. Thus, rectangular prisms modelled according to an on flat build orientation and 45° as raster angle exhibited a simulated frequency up to a 33% lower than the experimental frequency. Other internal configurations resulted in deviations higher than 13% in most cases (see Table 6).

Therefore, simulations based on internal geometry modelling were not successful in capturing the vibrational behavior of 3D

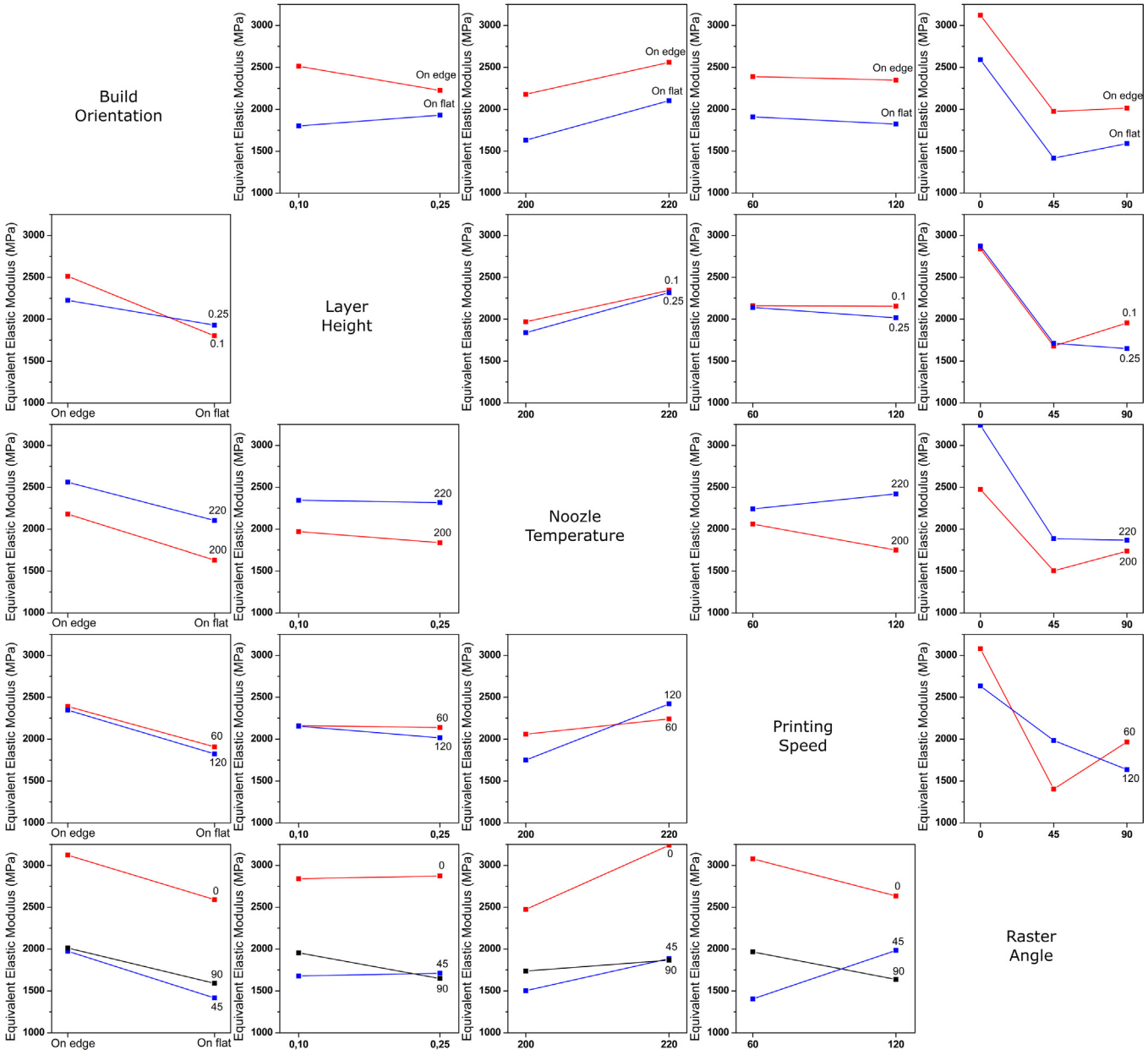

Fig. 8. Interaction graph showing interactions between 3D printing parameters.

Table 4
Combination of 3D printing fabrication parameters for the validation specimen group.

Number of specimens(n)	3D Printing parameters					Experimental Equivalent Elastic Modulus(MPa)	Predicted Equivalent Elastic Modulus(MPa)
	Build Orientation	Layer height (mm)	Nozzle Temperature (°C)	Printing Speed (mm/s)	Raster angle(°)		
2	On flat	0.175	210	90	0	1893 1941	2540
2	On flat	0.175	210	90	45	837 896	1385
2	On flat	0.175	210	90	90	1497 1345	1518

printed rectangular prisms, at least when the nominal elastic modulus of PLA (2346.5 MPa) was considered. More sophisticated finite element simulations may be necessary to capture properly the vibrational behavior of parts with the typical mesostructure generated by FFF. In this regard, the use of the equivalent elastic modulus in modal analysis simulations appears to be a simpler and more effective method to reproduce the experimental dynamic behavior.

Bearing in mind that the equivalent elastic modulus may be a useful property in finite element method simulations of 3D printed parts, our last purpose was to check the applicability of this metric

Table 5
Comparison between the experimental frequency of 3D printed prisms and the simulated frequency obtained using the predicted equivalent elastic modulus.

3D printing process parameter		Simulated Frequency (Hz)	Experimental Frequency (Hz)	Error(%)
Build Orientation	On Flat	81.3	78.7	−3.3
	On Edge	91.6	101.5	9.8
Layer Height(mm)	0.1	87.5	92.4	5.3
	0.25	85.8	87.6	2.1
Nozzle Temperature(°C)	200	82.2	84.5	2.7
	220	90.9	95.4	4.7
Printing Speed(mm/s)	60	87.3	89.6	2.6
	120	86.0	90.4	4.9
Raster Angle	0°	100.6	95.3	−5.6
	45°	77.5	84.8	8.6
	90°	79.9	90.0	11.2

Table 6
First mode shape frequencies corresponding to simulations based on the internal geometry modelling of 3D printed prisms.

				Simulated Frequency (Hz)	Experimental Frequency (Hz)	Error (%)
Build Orientation	On Flat	Raster Angle	0°	92.6	91.1	−1.6
			45°	46.3	69.3	33.3
			90°	63.3	75.6	16.3
	On Edge	Raster Angle	0°	72.3	99.8	27.6
			45°	73.6	100.2	26.6
			90°	90.7	104.4	13.2

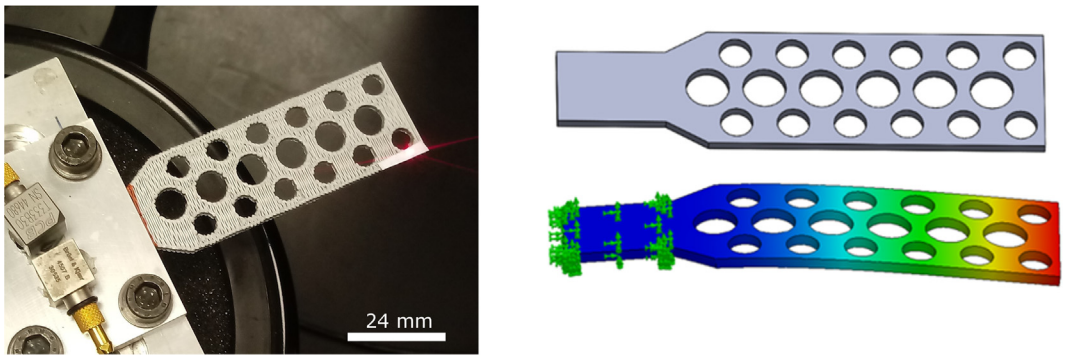

Fig. 9. Experimental set-up and dynamic behavior simulation results for a 3D printed multi tube support.

in the assessment of a more complex piece. In this case, a multi tube support was 3D printed on flat, using a layer height of 0.1 mm, a nozzle temperature of 200 °C, a printing speed of 120 mm/s and 90° as raster angle (see Fig. 9). The dynamic behavior of this part was characterized, finding the experimental frequency for the first mode shape: 51.5 Hz. Then, we compared the former experimental frequency with the frequencies obtained from simulations of the modal behavior using both the nominal elastic modulus for PLA (2346.5 MPa) and the equivalent elastic modulus predicted by the model (1208.5 MPa) for the prior 3D printing parameter combination. The latter gave a frequency for the first mode of 54.9 Hz, whereas the former yielded a frequency of 76.5 Hz, confirming the validity of the equivalent elastic modulus as a more realistic metric for use in simulations of the vibrational behavior of 3D printed parts.

This study had a number of limitations. First, our experimental plan did not include all the process parameters that intervene in FFF. Air gap, bed or envelope temperature, extruder diameter, infill density and number of shell perimeters, among others, were either not considered or they were set to default values. It is already known that air gap and infill density have significant effects on mechanical performance, with zero or negative air gaps and 100% solid infill densities preferred for superior mechanical properties [13,22,23,30,44]. On the other hand, smaller nozzle diameters imply longer fabrication times and they were associated with lower ultimate loads, according to Basgul and coworkers [9]. Second, our experimental plan included only two or three levels for most of the variables to make the study less time intensive. In this regard, our study would have needed more levels in the printing speed and layer thickness variables to capture more potentially significant influences on mechanical behavior. As reported earlier, low printing speeds may favor increased local heating and therefore fiber-to-fiber and interlayer bonding, whereas layer thicknesses equal or greater than the nozzle diameter may result in reduced contact areas between deposited filaments [21,31], having these phenomena important consequences from the mechanical point of view. Assuring a proper and more complete level selection, we anticipate laser-scanning vibrometry will discriminate the former effects based on the detection of significant influences and interactions in the present study. Finally, the third limitation of our study is that the modal analysis simulations performed, especially those based on internal geometry modelling, were based on too simplistic assumptions. Fused Filament Fabrication produces a typical mesostructure of bonded fibers and voids, which is far from being homogeneous as fiber-to-fiber bonds and interlayer bonds may have very different mechanical properties that the fiber core. Nevertheless, the predicted equivalent elastic modulus, which arose from our ad hoc model, was a useful metric in the modal analysis simulation of a more complex part, giving frequency values close to the experimental behavior. This methodology, 3D

printing production of coupons with specific process parameters and laser-scanning vibrometry characterization, may be applicable and useful in the design and production of complex, real-world, 3D printed parts with customized mechanical behavior.

4. Conclusions

In this study, laser-scanning vibrometry has proved successful in the mechanical characterization of 3D printed rectangular prisms. This technique has allowed identification of significant influences and interactions of 3D printing process parameters on the equivalent elastic modulus of 3D printed parts. Statistical analysis of the current dataset identified, from a mechanical perspective, linearly significant process parameters, namely raster angle, build orientation and nozzle temperature. In this sense, our results agree with the importance of the alignment of deposited fibers and loading direction for superior mechanical performance and the need for high enough nozzle temperature and longer cooling times to ensure optimal fiber-to-fiber and interlayer bonding. Moreover, using multivariate regression models, we were able to rank the influence of 3D printing process parameters on the equivalent elastic modulus of rectangular prisms produced by FFF. These models also served to confirm significant interactions (both quadratic and cubic) between process parameters, which in some cases exhibited higher significance than single 3D printing design parameters. For instance, the interaction printing speed*raster angle was much more significant than printing speed and layer thickness alone in this study. The previous knowledge was then applied to generate an ad hoc model selecting the more important factors (linear and interactions) within the 3D printing process parameters. This ad hoc model provided equivalent elastic modulus data that was used in further simulations of the modal behavior, giving results very close to the experimental ones ($\leq$11%). Based on our study, the use of laser-scanning vibrometry appears very promising in the characterization of the mechanical integrity and quality of 3D printed parts. Other additive manufacturing technologies may benefit from the use of this technique and from the adoption of the presented methodology to test, simulate and optimize the properties of 3D printed parts. Further research on the use of laser-scanning vibrometry for characterization of 3D printed specimens designed for different mechanical scenarios (torsion, compression, impact, fatigue, etc.) and for analysis of other mode shapes and damping properties is warranted.

CRediT authorship contribution statement

Francisco Medel: Conceptualization, Methodology, Formal analysis, Data curation, Writing - original draft, Writing - review & editing, Resources, Supervision. **Víctor Esteban:** Investigation, Formal analysis, Writing - review & editing. **Javier Abad:** Conceptualization, Methodology, Writing - review & editing, Resources, Supervision.

Declaration of Competing Interest

The authors declare that they have no known competing financial interests or personal relationships that could have appeared to influence the work reported in this paper.

Acknowledgements

This study was supported by grants (Grupo de Biomateriales T48_20R and Grupo VEHIVIAL T19_20R) from Diputación General de Aragón (Spain).

Data availability

The raw/processed data required to reproduce these findings cannot be shared at this time as the data also forms part of an ongoing study.

References

[1] W. Gao, Y.B. Zhang, D. Ramanujan, K. Ramani, Y. Chen, C.B. Williams, C.C.L. Wang, Y.C. Shin, S. Zhang, P.D. Zavattieri, The status, challenges, and future of additive manufacturing in engineering, Comput. Aided Des. 69 (2015) 65–89.
[2] B.N. Turner, R. Strong, S.A. Gold, A review of melt extrusion additive manufacturing processes: I. Process design and modeling, Rapid Prototyping J. 20 (3) (2014) 192–204.
[3] B.N. Turner, S.A. Gold, A review of melt extrusion additive manufacturing processes: II. Materials, dimensional accuracy, and surface roughness, Rapid Prototyping J. 21 (3) (2015) 250–261.
[4] R. Jones, P. Haufe, E. Sells, P. Iravani, V. Olliver, C. Palmer, A. Bowyer, RepRap - the replicating rapid prototyper, Robotica 29 (2011) 177–191.
[5] J. Yin, C.H. Lu, J.Z. Fu, Y. Huang, Y.X. Zheng, Interfacial bonding during multi-material fused deposition modeling (FDM) process due to inter-molecular diffusion, Mater. Des. 150 (2018) 104–112.
[6] M.S. Hossain, D. Espalin, J. Ramos, M. Perez, R. Wicker, Improved Mechanical Properties of Fused Deposition Modeling-Manufactured Parts Through Build Parameter Modifications, J. Manuf. Sci. Eng. –Trans. ASME 136 (6) (2014).
[7] C. Basgul, T. Yu, D.W. MacDonald, R. Siskey, M. Marcolongo, S.M. Kurtz, Structure-property relationships for 3D-printed PEEK intervertebral lumbar cages produced using fused filament fabrication, J. Mater. Res. 33 (14) (2018) 2040–2051.
[8] C. Basgul, T. Yu, D.W. MacDonald, R. Siskey, M. Marcolongo, S.M. Kurtz, Does annealing improve the interlayer adhesion and structural integrity of FFF 3D printed PEEK lumbar spinal cages?, J. Mech. Behav. Biomed. Mater. 102 (2020) 103455.
[9] C. Basgul, D.W. MacDonald, R. Siskey, S.M. Kurtz, Thermal Localization Improves the Interlayer Adhesion and Structural Integrity of 3D printed PEEK Lumbar Spinal Cages, Materialia (Oxf) 10 (2020).
[10] L. Boldrin, S. Hummel, F. Scarpa, D. Di Maio, C. Lira, M. Ruzzene, C.D.L. Remillat, T.C. Lim, R. Rajasekaran, S. Patsias, Dynamic behaviour of auxetic gradient composite hexagonal honeycombs, Compos. Struct. 149 (2016) 114–124.
[11] J.G. Lopes, C.M. Machado, V.R. Duarte, T.A. Rodrigues, T.G. Santos, J.P. Oliveira, Effect of milling parameters on HSLA steel parts produced by Wire and Arc Additive Manufacturing (WAAM), J. Manuf. Processes 59 (2020) 739–749.
[12] S.H. Ahn, M. Montero, D. Odell, S. Roundy, P.K. Wright, Anisotropic material properties of fused deposition modeling ABS, Rapid Prototyping J. 8 (4) (2002) 248–257.
[13] A. Rodriguez-Panes, J. Claver, A.M. Camacho, The Influence of Manufacturing Parameters on the Mechanical Behaviour of PLA and ABS Pieces Manufactured by FDM: A Comparative Analysis, Materials 11 (8) (2018).
[14] J.P. Oliveira, A.D. LaLonde, J. Ma, Processing parameters in laser powder bed fusion metal additive manufacturing, Mater. Des. 193 (2020) 12.
[15] O.A. Mohamed, S.H. Masood, J.L. Bhowmik, Optimization of fused deposition modeling process parameters: a review of current research and future prospects, Adv. Manuf. 3 (1) (2015) 42–53.
[16] D. Popescu, A. Zapciu, C. Amza, F. Baciu, R. Marinescu, FDM process parameters influence over the mechanical properties of polymer specimens: A review, Polym. Test. 69 (2018) 157–166.
[17] J.R.C. Dizon, A.H. Espera, Q.Y. Chen, R.C. Advincula, O Mechanical characterization of 3D-printed polymers, Addit. Manuf. 20 (2018) 44–67.
[18] J.M. Chacon, M.A. Caminero, E. Garcia-Plaza, P.J. Nunez, Additive manufacturing of PLA structures using fused deposition modelling: Effect of process parameters on mechanical properties and their optimal selection, Mater. Des. 124 (2017) 143–157.
[19] S. Shaffer, K.J. Yang, J. Vargas, M.A. Di Prima, W. Voit, On reducing anisotropy in 3D printed polymers via ionizing radiation, Polymer 55 (23) (2014) 5969–5979.
[20] Y. Song, Y. Li, W. Song, K. Yee, K.Y. Lee, V.L. Tagarielli, Measurements of the mechanical response of unidirectional 3D-printed PLA, Mater. Des. 123 (2017) 154–164.
[21] A.C. Abbott, G.P. Tandon, R.L. Bradford, H. Koerner, J.W. Baur, Process-structure-property effects on ABS bond strength in fused filament fabrication, Addit. Manuf. 19 (2018) 29–38.
[22] A.K. Sood, R.K. Ohdar, S.S. Mahapatra, Parametric appraisal of mechanical property of fused deposition modelling processed parts, Mater. Des. 31 (1) (2010) 287–295.
[23] S. Ziemian, M. Okwara, C.W. Ziemian, Tensile and fatigue behavior of layered acrylonitrile butadiene styrene, Rapid Prototyping J. 21 (3) (2015) 270–278.
[24] C.W. Ziemian, R.D. Ziemian, K.V. Haile, Characterization of stiffness degradation caused by fatigue damage of additive manufactured parts, Mater. Des. 109 (2016) 209–218.
[25] M. Domingo-Espin, J.M. Puigoriol-Forcada, A.A. Garcia-Granada, J. Lluma, S. Borros, G. Reyes, Mechanical property characterization and simulation of fused deposition modeling Polycarbonate parts, Mater. Des. 83 (2015) 670–677.
[26] C. Casavola, A. Cazzato, V. Moramarco, C. Pappalettere, Orthotropic mechanical properties of fused deposition modelling parts described by classical laminate theory, Mater. Des. 90 (2016) 453–458.

[27] D.W. Abueidda, M. Elhebeary, C.S. Shiang, S.Y. Pang, R.K. Abu Al-Rub, I.M. Jasiuk, Mechanical properties of 3D printed polymeric Gyroid cellular structures: Experimental and finite element study, Mater. Des. 165 (2019).
[28] B.M. Tymrak, M. Kreiger, J.M. Pearce, Mechanical properties of components fabricated with open-source 3-D printers under realistic environmental conditions, Mater. Des. 58 (2014) 242–246.
[29] A.G. Salazar-Martin, M.A. Perez, A.A. Garcia-Granada, G. Reyes, J.M. Puigoriol-Forcada, A study of creep in polycarbonate fused deposition modelling parts, Mater. Des. 141 (2018) 414–425.
[30] G. Gomez-Gras, R. Jerez-Mesa, J.A. Travieso-Rodriguez, J. Lluma-Fuentes, Fatigue performance of fused filament fabrication PLA specimens, Mater. Des. 140 (2018) 278–285.
[31] N. Aliheidari, J. Christ, R. Tripuraneni, S. Nadimpalli, A. Ameli, Interlayer adhesion and fracture resistance of polymers printed through melt extrusion additive manufacturing process, Mater. Des. 156 (2018) 351–361.
[32] C. Bellehumeur, L. Li, Q. Sun, P. Gu, Modeling of Bond Formation Between Polymer Filaments in the Fused Deposition Modeling Process, J. Manuf. Processes 6 (2) (2004) 170–178.
[33] O.A. Mohamed, S.H. Masood, J.L. Bhowmik, Analytical Modelling and Optimization of the Temperature-Dependent Dynamic Mechanical Properties of Fused Deposition Fabricated Parts Made of PC-ABS, Materials 9 (11) (2016).
[34] J. Lee, A. Huang, Fatigue analysis of FDM materials, Rapid Prototyping J. 19 (4) (2013) 291–299.
[35] D.A. Turk, F. Brenni, M. Zogg, M. Meboldt, Mechanical characterization of 3D printed polymers for fiber reinforced polymers processing, Mater. Des. 118 (2017) 256–265.
[36] E. Kozin, N. Black, J. Cheng, M. Cotler, M. McKenna, D. Lee, J. Lewis, J. Rosowski, A. Remenschneider, Design, fabrication, and in vitro testing of novel three-dimensionally printed tympanic membrane grafts, Hear. Res. 340 (2016) 191–203.
[37] A.V. Filippov, V.A. Krasnoveikin, N.V. Druzhinin, V.E. Rubtsov, The Use of Laser-Doppler Vibrometry for Modal Analysis of Carbon-Fiber Reinforced Composite, Key Eng. Mater. 712 (2016) 313–318.
[38] S.S. Rao, Mechanical Vibrations, Pearson/Prentice Hall, 2004.
[39] W.C. Young, R.G. Budynas, R.J. Roark, Roark's formulas for stress and strain, McGraw-Hill, New York; London, 2002.
[40] R. Gautam, S. Idapalapati, S. Feih, Printing and characterisation of Kagome lattice structures by fused deposition modelling, Mater. Des. 137 (2018) 266–275.
[41] C. Kousiatza, D. Karalekas, In-situ monitoring of strain and temperature distributions during fused deposition modeling process, Mater. Des. 97 (2016) 400–406.
[42] J.R. Sarasua, A.L. Arraiza, P. Balerdi, I. Maiza, Crystallinity and mechanical properties of optically pure polylactides and their blends, Polym. Eng. Sci. 45 (5) (2005) 745–753.
[43] A. Lanzotti, M. Grasso, G. Staiano, M. Martorelli, The impact of process parameters on mechanical properties of parts fabricated in PLA with an open-source 3-D printer, Rapid Prototyping J. 21 (5) (2015) 604–617.
[44] K.C. Ang, K.F. Leong, C.K. Chua, M. Chandrasekaran, Investigation of the mechanical properties and porosity relationships in fused deposition modelling-fabricated porous structures, Rapid Prototyping J. 12 (2) (2006) 100–105.